On quantum transport in flat-band materials

Oriekhov, D.

Chapter 1

Introduction

1.1 Preface

This thesis is devoted to the study of the role of flat bands in transport and interacting properties of atomically-thin materials.

Flat band is defined as a part of Bloch band with macroscopically large region of momentum space with nearly constant dispersion. Why the flat bands are so important? The answer is given by considerations coming from classical physics (mechanics, electrodynamics). The equations of motion for a single particle in external potential U are captured by the Lagrangian function $L = T - U$ or Hamiltonian $H = T + U$ with T being a kinetic energy. The definition of flat band says that T is approximately constant in some parameter range - region in momentum space. Adjusting the energy level to this constant level $\tilde{T} = T - T_0$, we find that $\tilde{L} = \tilde{T} - U \approx U$. This means that the physics of a particle are determined solely by an external potential. Such situation in not typical for classical physics. The clear consequence of this estimation appears in quantum systems: even weak potential or interactions inside the system lead to instability of the initial ground state and re-configuration. In the modern experiments the investigation of possible new ground states in a flat band systems is a young topic which appeared just 5 years ago with a discovery of magic angle twisted bilayer graphene [1]. Nevertheless, the enormous attention led to appearance of many thousands of papers with number of intriguing results. The most prominent examples are discoveries of superconductivity and Mott insulating states in magic angle twisted bilayer [1] and trilayer [2], superconducting states in Bernal bilayer [3] and ABC trilayer graphene

[4], and Kagome metals [5].

In this thesis several theoretical predictions for the new ground states in flat band systems are discussed. One might ask why the ground state of flat band systems is so hard to calculate? The reason is that the presence of flat band enhances the role of *all* interactions. Thus, a very rigorous symmetry analysis and precise estimation of each of interaction constants is required to build a phase diagram and understand which phase dominates. In the Chapter 2 the strong enhancement of RKKY spin-spin interactions is predicted. For the case when the screened Coulomb interaction is present, the possibility of formation of excitonic gap with intervalley-polarized order is discussed in Chapter 3. These results can be viewed as a building blocks for future theory of phase diagram in flat band materials. Based on experiments like [1, 6] it is expected that one would have the competition between all these correlated states, and as an example the final ground state might have unconventional type of superconductivity. Also the high controllability in experiments with 2D materials might allow to tune and select which of interactions will be dominating in particular setup. Other main chapters of this thesis are devoted to the study of the role of flat bands in a non-interacting case. Such situation is typical for realizations of flat band materials in artificial systems such as STM-type experiments with electronic lattices [7], optical lattice realizations [8] or superlattice structures in organic chemical frameworks [9, 10].

1.2 Examples of simple tight-binding models with flat bands

Next, let us introduce the particular examples of flat band models studied in this thesis. The main idea behind these lattices is that they have simple geometry and the tight-binding description gives simple Hamiltonians that can be analyzed with analytical and numerical methods. The two lattices, dice and Lieb, discussed below are examples of bipartite lattices where connection between two different sublattices is made only via hopping parameters to third sublattice.

1.2.1 Dice lattice and $\alpha - \mathcal{T}_3$ model

The dice (also called $\mathcal{T}_3$) lattice is probably historically the first tight-binding model with flat bands. It was firstly studied by B. Sutherland

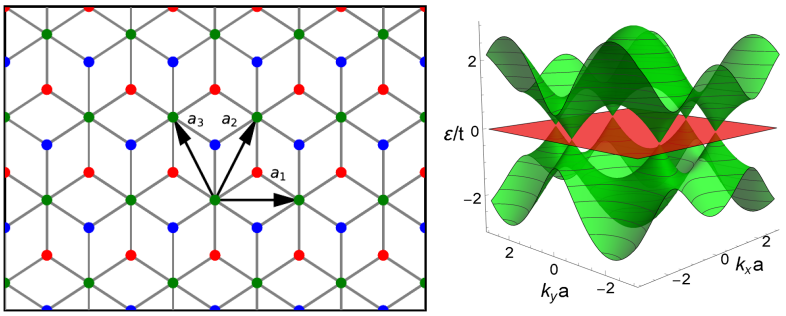

Figure 1.1. The dice (also called $\mathcal{T}_3$) lattice whose red points display atoms of the A sublattice, blue points describe the B sublattice, and the green points define the C sublattice. The vectors $\boldsymbol{a}_1 = (\sqrt{3},\, 0)d$ and $\boldsymbol{a}_2 = (\sqrt{3}/2,\, 3/2)d$ are the basis vectors of the C sublattice. The nearest neighbor hopping parameters between hub (C) and rim (A, B) atoms are t_1 and t_2.

in 1986 [11] as an example where localization of wave functions happens due to local topology. The $\alpha - \mathcal{T}_3$ model describes quasiparticles in two dimensions on the dice lattice schematically shown in Fig.1.1, where d denotes the distance between neighbor atoms. This lattice has a unit cell with three different lattice sites whose two sites (A, C) like in graphene form a honeycomb lattice with hopping amplitude $t_{AC} = t_1$ and additional B sites at the center of each hexagon are connected to the C sites with hopping amplitude $t_{BC} = t_2$. The C atoms are called hub centers, while A and B are rim sites, and electrons hop between rim and hub atoms only. Two hopping parameters t_1 and t_2 are not equal, in general, and the dice model corresponds to the limit $t_1 = t_2$. The lattice structure and basis vectors $\mathbf{a}_1 = (\sqrt{3}, 0)d$, $\mathbf{a}_2 = (\sqrt{3}/2, 3/2)d$ are shown on Fig.1.1. Since there are three atoms per unit cell, the wave functions can be written in terms of 3-component vectors with elements assigned to each sublattice. This leads to the so-called pseudospin $S = 1$ description.

The tight-binding equations are [12]:

$$\begin{aligned}
\varepsilon\Psi_C(\boldsymbol{r}) &= -t_1 \sum_j \Psi_A(\boldsymbol{r} + \boldsymbol{\delta}_j^A) - t_2 \sum_j \Psi_B(\boldsymbol{r} - \boldsymbol{\delta}_j^A), \\
\varepsilon\Psi_A(\boldsymbol{r}) &= -t_1 \sum_j \Psi_C(\boldsymbol{r} - \boldsymbol{\delta}_j^A), \\
\varepsilon\Psi_B(\boldsymbol{r}) &= -t_2 \sum_j \Psi_C(\boldsymbol{r} + \boldsymbol{\delta}_j^A),
\end{aligned} \tag{1.1}$$

where the vectors δ_j^A connect nearest neighbor atoms C to atoms A:

$$\boldsymbol{\delta}_1^A = \frac{\mathbf{a}_1 + \mathbf{a}_2}{3},\ \boldsymbol{\delta}_2^A = \frac{\mathbf{a}_3 - \mathbf{a}_1}{3},\ \boldsymbol{\delta}_3^A = -\frac{\mathbf{a}_2 + \mathbf{a}_3}{3} \quad \text{with} \quad \mathbf{a}_3 = \mathbf{a}_2 - \mathbf{a}_1. \tag{1.2}$$

The corresponding tight-binding Hamiltonian in momentum space reads [13]

$$H_0(\boldsymbol{k}) = \begin{pmatrix} 0 & f_{\boldsymbol{k}} \cos\Theta & 0 \\ f_{\boldsymbol{k}}^* \cos\Theta & 0 & f_{\boldsymbol{k}} \sin\Theta \\ 0 & f_{\boldsymbol{k}}^* \sin\Theta & 0 \end{pmatrix}, \quad \alpha \equiv \tan\Theta = \frac{t_2}{t_1},$$
$$f_{\boldsymbol{k}} = -\sqrt{t_1^2 + t_2^2}\,(1 + e^{-i\boldsymbol{k}\boldsymbol{a}_2} + e^{-i\boldsymbol{k}\boldsymbol{a}_3}), \tag{1.3}$$

and acts on three-component wave functions with the following order of components $\Psi^T = (\Psi_A, \Psi_C, \Psi_B)$. As was noted in Introduction, the angle Θ can be used to interpolate between graphene and dice model. Thus, our results can be compared with graphene literature by taking limit $\Theta \to 0$ or $\Theta \to \frac{\pi}{2}$.

It is easy to derive the energy spectrum of the above Hamiltonian, which is qualitatively the same for any α and consists of three bands: the zero-energy flat band, $\varepsilon_0(\mathbf{k}) = 0$, whose existence is protected by the particle-hole symmetry, and two dispersive bands

$$\varepsilon_\pm(\mathbf{k}) = \pm|f_k| = \pm\sqrt{t_1^2 + t_2^2}\Big[3 + 2(\cos(\boldsymbol{a}_1\boldsymbol{k}) + \cos(\boldsymbol{a}_2\boldsymbol{k}) + \cos(\boldsymbol{a}_3\boldsymbol{k}))\Big]^{1/2}. \tag{1.4}$$

The eigenvectors in the whole Brillouin zone (BZ) are given by Eq.(2) in [13] (gapless case) and by Eq.(5) in [14] (gapped case). For dispersionless band the wave function is localized on atoms of sublattices A, B while it is zero on hub atoms C. The presence of a completely flat band with zero energy is perhaps one of the remarkable properties of the $\alpha - \mathcal{T}_3$ lattice model.

There are six values of momentum for which $f_{\boldsymbol{k}} = 0$ and all three bands intersect. They are situated at corners of the hexagonal Brillouin zone. The two inequivalent points, for example, are

$$\boldsymbol{K} = \frac{2\pi}{d}\left(\frac{\sqrt{3}}{9}, \frac{1}{3}\right), \quad \boldsymbol{K}' = \frac{2\pi}{d}\left(-\frac{\sqrt{3}}{9}, \frac{1}{3}\right). \tag{1.5}$$

For momenta near the K-points, $\boldsymbol{k} = \boldsymbol{K}(\boldsymbol{K}') + \tilde{\boldsymbol{k}}$, we find that $f_{\boldsymbol{k}}$ is linear in $\tilde{\boldsymbol{k}}$, i.e., $f_{\boldsymbol{k}} = \hbar v_F(\xi\tilde{k}_x - i\tilde{k}_y)$ with valley index $\xi = \pm$, where $v_F = 3td/2\hbar$ is the Fermi velocity, and in what follows we omit for the simplicity of notation the tilde over momentum. As for lattice parameters we take their numerical values the same as in graphene. Hence, in the linear order to momentum deviations from the K and K' points, the low-energy Hamiltonian describes massless pseudospin-1 fermions [12, 13] which for equal hoppings, $\Theta = \pi/4$, is given by the scalar product of momentum and the spin-1 matrices:

$$H_\xi(\mathbf{k}) = \hbar v_F \left(\xi S_x k_x + S_y k_y\right), \\ S_x = \frac{1}{\sqrt{2}} \begin{pmatrix} 0 & 1 & 0 \\ 1 & 0 & 1 \\ 0 & 1 & 0 \end{pmatrix}, \quad S_y = \frac{1}{\sqrt{2}} \begin{pmatrix} 0 & -i & 0 \\ i & 0 & -i \\ 0 & i & 0 \end{pmatrix} \tag{1.6}$$

where $\mathbf{k} = \mathbf{q} - \mathbf{K}_\xi$ is the wave vector measured relative to the Dirac points located at $\mathbf{K}_\xi = \xi 4\pi/(3\sqrt{3}a)\,\{1, 0\}$, corresponding to K ($\xi = +$) and K' ($\xi = -$) points, and $v_F = 3ta/(\sqrt{2}\hbar)$ is the Fermi velocity. This Hamiltonian reminds a Dirac-type Hamiltonian (relativistic dispersion) but now for spin-1 particles. Such effective Hamiltonians, that do not occur for elementary particles in high-energy physics, attracted much attention in the last years [15].

The $\mathcal{T}_3$ lattice was experimentally realized in Josephson arrays [16, 17] as well as in a network made of metallic wires tailored in a high mobility two-dimensional electron gas [18], and its optical realization by laser beams was proposed in Ref.[19]. The atomic-scale realization of dice lattice is missing because of the complexity of hopping structure (the hoppings between neighboring A and B sublattices should be strongly suppressed).

1.2.2 Lieb lattice

The Lieb lattice is schematically shown in Fig.1.2. It was studied by E. H. Lieb in 1989 [20] in connection with specific properties of Heisenberg spin model on it. This lattice consists of three square sublattices, with atoms placed in the corners and in the middle of each side of big squares forming a line-centered-square lattice. The tight-binding equations describing this lattice are very similar to Eq.(1.1), the only difference comes from the orientation of vectors connecting nearest neighbors δ_j. The tight-binding

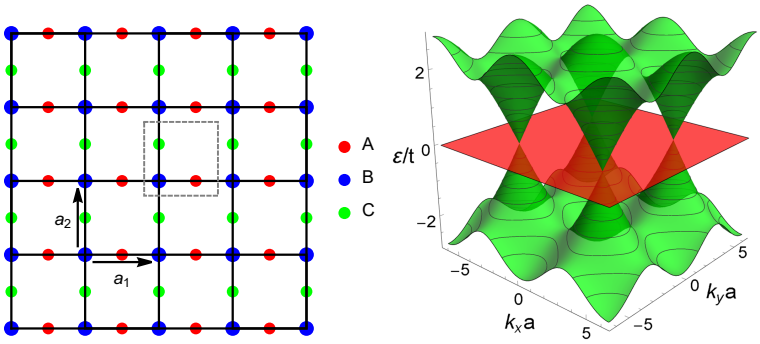

Figure 1.2. The Lieb lattice whose red points display atoms of the A sublattice, blue points describe the B sublattice, and the green points define the C sublattice. The vectors $\boldsymbol{a}_1 = (1, 0)a$ and $\boldsymbol{a}_2 = (0, 1)a$ are the basis vectors of the B sublattice. The nearest neighbor hopping parameters between hub (B) and rim (A, C) atoms are t_1 and t_2.

Hamiltonian was described in Ref.[21]:

$$H_0 = \begin{pmatrix} 0 & -2t\cos(k_x a/2) & 0 \\ -2t\cos(k_x a/2) & 0 & -2t\cos(k_y a/2) \\ 0 & -2t\cos(k_y a/2) & 0 \end{pmatrix} \tag{1.7}$$

Notably, the dispersion contains only single Dirac cone inside first Brillouin zone (see Fig.1.2). This Hamiltonian reduces to the following low-energy model near the center of BZ $k_{x,y} = \frac{\pi}{a} + q_{x,y}$:

$$H_{Lieb} = \begin{pmatrix} 0 & v_F q_x & 0 \\ v_F q_x & 0 & v_F q_y \\ 0 & v_F q_y & 0 \end{pmatrix}. \tag{1.8}$$

The energy dispersions defined by this Hamiltonian are given by three bands, one is flat band and the other two are dispersive bands (see Fig.4.4c):

$$\varepsilon_0 = 0, \ \varepsilon_\pm = \pm 2t\sqrt{\cos^2(k_x a/2) + \cos^2(k_y a/2)}. \tag{1.9}$$

The notable property of both dice and Lieb lattices in that flat band is placed at charge-neutrality point. Below we discuss the structure of wave functions in flat band in real space.

The experimental realization of Lieb lattice on atomic scale was made with the help of STM technique that creates an electronic lattice on surface of substrate [7].

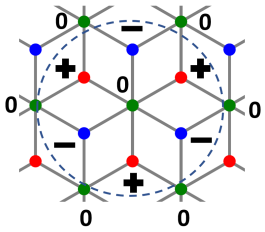

Figure 1.3. The configuration of flat band state wave function that is localized around one of the hub sites. While the components of the wave function on a hub (green C) sites are zeros, the sign-alternating components on A and B sites compose a localized state.

1.2.3 Structure of flat band wave functions on a lattice

The main feature of the models described above in the presence of exactly flat band at the charge-neutrality point in the spectrum. it is easy to find flat band solutions in momentum space from tight-binding Hamiltonian. But the question arises - how such states are organized on a lattice? The answer on this question was the historical motivation that attracted attention to these lattices [11, 20] well before the first atomically-thin material was experimentally realized [22].

Let us look on tight-binding equations (1.1). The flat band placed at zero energy results in three equations:

$$0 = -t_1 \sum_j \Psi_A(\boldsymbol{r} + \boldsymbol{\delta}_j^A) - t_2 \sum_j \Psi_B(\boldsymbol{r} - \boldsymbol{\delta}_j^A),$$
$$0 = -t_1 \sum_j \Psi_C(\boldsymbol{r} - \boldsymbol{\delta}_j^A), \quad 0 = -t_2 \sum_j \Psi_C(\boldsymbol{r} + \boldsymbol{\delta}_j^A). \tag{1.10}$$

The two last equations are equivalent and give the same solution $\Psi_C(\boldsymbol{r}) = 0$. The first equation gives algebraic relation on components of wave function on A and B sublattices, that can be easily satisfied by choosing the sign structures of the components according to the Fig.1.3. For example, all B-components are equal to $\Psi_B = -t_1/t_2 \Psi_A$. The state shown in Fig.1.3 is localized around one of the sublattice C sites. For each site one can build correspond state, thus having the high degeneracy of such flat band of the order of number of atoms in the sample. The experiments [16–18] have confirmed the existence of novel localization effects, which arise due to the presence of flat band in the spectrum of $\mathcal{T}_3$ lattice.

1.3 Beyond exactly flat bands: high-order van Hove singularities

In experiments with atomically-thin crystals it is typical to have not exactly flat bands due to different next nearest neighbor hopping terms, role of substrates and similar effects [1, 23]. The general concept that captures relatively "flat" parts of band in a dispersion are called saddle points. The corresponding pronounced divergent peaks in density of states are called van Hove singularities. The original concept was studied by L. van Hove in 1953 [24]. Recently, a generalization of the concept, called high-order van Hove singularities, was introduced by Liang Fu group [25]. The difference between these concepts is the following:

1) The term "flat bands" in this Thesis is used to describe bands that have constant dispersion, thus representing mathematically precise flatness of the band. The corresponding density of states has a Dirac delta-function peak;

2) the usual van Hove singularities correspond to momentum-dependent dispersion $\varepsilon(k_x, k_y) \sim k_x^2 - k_y^2$ and give logarithmically-divergent density of states;

3) the high-order van Hove singularities give power law divergent density of states.

All such features in the band structure are expected to produce strongly correlated states (superconductivity, etc) at corresponding doping due to high density of states and small group velocity of quasiparticles [26–28]. However, some observable signatures might be different and the Sixth Chapter 6 studies such differences for orbital susceptibility. The classification of high-order van Hove singularities was given in Refs.[29, 30], and the field of discovering materials with them only starts its growing.

1.4 Zero energy modes: Majorana zero modes and Andreev bound states

When the flat band is placed close to charge-neutrality point in the system the whole reach physical picture coming from flat bands becomes easily accessible for experimental studies. In addition to discussion of possible physical effects related to the flat bands in 2D crystals, this thesis also contains several results related to another type of states placed

near charge-neutrality point: Majorana zero modes and Andreeev bound states.

In the past decades the great attention was given to a possibility of making topologically protected quantum qubit. One of the key possibilities was to use so-called Majorana zero modes - a collective excitations in superconductors that are bound to zero energy (charge neutrality point) and are non-Abelian anions.

However, they are typically mimicked by another non-topological modes placed at or around charge neutrality point - Andreeev bound states. Such bound states appear in Josephson junctions. In this case mimicking means that the expected observable signatures of Majorana zero modes are nearly exactly reproduced by Andreev bound states.

Modern experimental state of this is the following: there are devised that host Majorana modes, however their manufacturing is related to enormously complicated process of reducing disorder [31]. Still a next generation of experiments is required to make Majorana zero modes accessible for quantum computing.

In this thesis chapters 7 and 8 are devoted to Majorana zero modes and the signatures mimicked by Andreev bound states.

1.5 About this thesis

Below follows the brief description of chapter contents:

1.5.1 Chapter 2

The Second chapter is devoted to the study of spin-spin interaction between two impurities placed on a 2D dice lattice. Such interaction is mediated by the electrons of a lattice. It is called Ruderman-Kittel-Kasuya-Yoshida [32–34] spin-spin interaction. The RKKY interaction was calculated using the effective low-energy theory that works close to charge-neutrality point and captures flat band and Dirac cones. The standard approximation of RKKY interaction which uses non-interacting Green's function of the electrons was used. The main results concerning the role of flat band are the following: the RKKY interaction between two impurities is strongly enhanced and diverges as inverse temperature when chemical potential placed at flat band level. At the same time enhancement is finite but large when the chemical potential is close to flat band

level. Such picture holds only for certain positions of impurities related to the localization of flat band wave functions. Apart from that, the description of the RKKY interaction for arbitrary temperatures and positions of chemical potential are given in terms of exact analytic expressions.

Apart from that, the chapter contains important mathematical results for the physics of RKKY interaction in graphene. The interaction integrals are calculated in the most general fashion with both finite temperature and chemical potential taken into account. The exact analytic expressions obtained there allow one to analyze dependencies on physical parameters and relative positions of impurities on different sublattices as well as obtain short exponentially-precise asymptotic expressions.

1.5.2 Chapter 3

In the Third Chapter the role of flat band in dynamical generation of excitonic gap is studied. Excitons are bound states of electron and holes tied by an attractive Coulomb interaction. The excitonic gap in the spectrum appears when it is energetically favorable to create excitons out of electrons and holes that have energies close to charge-neutrality point. Experimentally and theoretically it was found that the excitonic gap is generated in multilayer graphene (see Refs.[35–44]) and the more softer dispersion is - the larger gap is generated. Such picture is in agreement with simple considerations about the role of kinetic and potential energies discussed in the Preface (1.1) of this Introduction.

As the flat bands represent the most soft type of kinetic energy, it is expected that the dynamical excitonic gap generation should be favorable. In the Chapter 3 several possible gap parameters for dice lattice are studied that satisfy symmetries and correspond to different pairings in sublattice spaces. It is shown that among several possible scenarios one dominates as energetically more favorable. The excitonic gap in such case has an intervalley type (pairing happens for quasiparticles from different valleys). For the formation of corresponding order parameter (excitonic gap) the flat band plays a role of catalyst. Similarly to chemical reactions, where the catalyst does not disappear during reaction but helps it to proceed more efficiently, the excitonic gap formation splits flat band into two but leaves both of them perfectly flat. But, the flat band enormously enhances the energy gap size. These predictions suggest that such mechanism might compete with superconductivity in flat band systems and dominate in their transport properties at intermediate temperatures

leading to insulating state.

In addition, it is important to underline that the type of excitonic gap that is favorable due to flat band catalysis has particular type of symmetry. In other words, not every type of excitonic order parameter is enhanced in the presence of flat band. The studies of such valley-mixing order parameters in more complicated systems such as twisted bilayer graphene are very active ongoing topic [45, 46].

1.5.3 Chapter 4

In the Fourth Chapter of this thesis the role of flat bands in the optical properties of dice and Lieb lattices was analyzed. For this purpose a zitterbewegung method, firstly introduced by J. Cserti et.al. [47], was generalized to be used for different effective models.

The calculation of optical conductivity is based on a Kubo formula for linear response. However, for most typical models the analytical calculations quickly become very complicated and the full integration cannot be performed. The idea behind zitterbewegung method is to convert part of calculation complexity into solution of differential equations - Heisenberg equations of motion. For particles with positive and negative energy bands in spectrum such equations predict a trembling motion, zitterbewegung (firstly discovered by Schrödinger in 1930 [48]). Trembling motion in this case means that the position of free propagating wave packet performs oscillations with very small amplitude and high frequency.

In the case of optical conductivity the solutions of Heisenberg equations and proper substitution of results into current response correlators allowed to perform full calculation for a number of effective models. In the Fourth Chapter we firstly analyzed the optical conductivity of semi-Dirac model where the Dirac cones can move with varying parameters of the model and merge into one. The obtained exact expressions capture the contributions of different transitions into optical condctivity. In particular, the role of anisotropy and contribution of transitions between van Hove singularities into the high peaks in conductivity were shown. In addition, the dice and Lieb flat band models were studied. Notably, the flat bands always support transitions from the dispersive bands, but in the case of dice model no transitions between two dispersive bands are allowed [49]. This is in contrast to what is found for the Lieb lattice in Chapter Four.

Additional mathematical result in the Chapter is that the zitterbewe-

gung method can be applied to effective models with complicated matrix algebras. This enhances the potential applicability of a method to new systems with other pseudospin structures frequently uncovered in last years [15].

1.5.4 Chapter 5

The Fifth Chapter is devoted to the study of bilayer dice lattices. As it is known from experiments, the different stackings of the same single-atom-thick lattices give the systems with very different properties. The most prominent example is the twisted bilayer graphene [1], where the proper rotation angle between layers allowed to achieve superconductivity. The idea of the Fifth Chapter is to study more simple stackings of two identical dice lattices with different sublattices aligned on top of each other. Since the dice lattice itself has flat band in spectrum and thus contains the pseudospin-1 fermions as effective quasiparticles, it is interesting to see whether bilayer configuration would preserve such quasiparticles.

The results of the Chapter show that while the triply degenerate points are always preserved, the effective dispersion of quasiparticles might change. The classification of all commensurate simple stackings is performed and it is shown that one can achieve pseudospin-1, semi-Dirac type of dispersion (with different dispersion law - linear and quadratic depending on direction) or nodal line crossings where two bands cross each other along high-symmetry line. Also the triple points are shifted from the charge-neutrality points, which means that the pseudospin-1 quasiparticles would be accessible upon doping. The results of this Chapter show how reach physics one could obtain out of bilayer stacking of a very simple flat band model.

The studies of such multilayer systems might explain how the properties of underlying simple flat band models result in nontrivial physics observed in more complicated crystals. As an example, one could think about Kagome metals where the perfect flat-band lattice is placed as a layer of 3D crystal [23] and several such layers separated from each other are present in chemically-stable order in a sample.

1.5.5 Chapter 6

In the Sixth Chapter the discussion about the role of flat bands in magnetic properties of 2D crystals is extended to the case of high-order van

Hove singularities. As it was shown in the literature, the usual van Hove singularities lead to paramagnetic response of the system [50], the exactly flat bands in the dice lattice lead to very strong paramagnetic response [13]. The corresponding paramagnetic response is manifestedvi a Dirac delta-function shape of the orbital susceptibility as function of chemical potential. Notably, in dice lattice this paramagnetic response dominates the diamagnetic Delta-like response of Dirac cones, which was present in graphene [51].

The focus of the Chapter is concentrated on studying the role of not perfectly flat bands - high-order van Hove singulatiries, in orbital susceptibility. As an example, the square-octagon lattice is analyzed. Such lattice was expected to occur as a stable 2D graphene allotrope - T-graphene, [52], but now is studied in connection with transition-metal dichalcogenides [53]. The chapter contains detailed characterization of tight-binding model describing square-octagon lattice, effective models that have form of 1) relativistic pseudospin-1 type and 2) second-order that capture precisely dispersion of high-order saddle point. Based on these models it is shown that paramagnetic contribution from van Hove singularity is weaker than that of flat band. The numerical calculations of orbital susceptibility show that the para-to-diamagnetic phase transition is possible if the parameters of the system are tuned.

The results on orbital susceptibility presented in the chapter show that magnetic properties of van Hove singularities of different kinds are more complicated that for exactly flat bands, and the full analysis of their role in orbital susceptibility for the novel 2D materials should be performed in future.

Next follow the additional chapters that are not focused on flat bands, but are related to zero-energy modes.

1.5.6 Chapter 7

This is the first out of two chapters devoted to the study of the Majorana zero modes and Andreev bound states. The topic of this Chapter is focused on the ways of distinguishing Majorana zero modes from Majorana fermions via transport experiments.

Majorana fermions in superconductors are coherent superpositions of electrons and holes. At the same time, Majorana zero modes are collective modes related to the winding of superconducting phase field by 2π that form a vortex. Such vortex typically contains bound state at zero energy,

which is called Majorana zero mode (MZM). While Majorana fermions satisfy usual Fermi-Dirac statistics, the MZMs satisfy non-Abelian anyon statistics. The transport of MZMs is governed by edge vortices that are domain walls with phase jump π on the boundary of superconductor.

As a way to distinguish these two "Majoranas" from each other, the measurement of shot noise in two similar devices (see Fig.7.1) is proposed. The shot noise power is calculated as a charge variance per injected single electron charge. For the Majorana fermion the result is known [54] ans constitutes e^2 per injected fermion. For MZM it is found to be dependent on the separation between two vortices on the edge. Thus, the shot noise has a nonlocal nature that signatures about long-range correlations between vortices. As an experimentally measurable consequence, the voltage dependence of shot noise can be used: for Majorana fermions shot noise increases linearly with growing voltage V, while for MZM it grows as $V \log V$.

1.5.7 Chapter 8

The Eighth Chapter is devoted to the study of effect that happens very similarly for Andreev bound states and Majorana modes. This effect, firstly predicted by S-J. Choi et.al. [55] in 2020 for Majorana qubit, is manifested as appearance of sharp voltage steps in the current-voltage characteristic for DC current injected into resistively-shunted junction with qubit. Notably, while Josephson junctions with quantum dots were studied experimentally for many decades, such effect was found only now.

However, it is known that Andreev levels close to charge-neutrality point typically mimic the behavior of topological qubits with Majorana modes. The study in the Chapter is performed for current-biased, resistively shunted quantum-dot Josephson junction. One of the key properties of this system is the existence of resonant state on the quantum dot. Such state leads to the appearance of particle-hole symmetric pair of Andreev bound states with finite lifetime. The existence of gaps separating these bound states from continuum of states in superconductors and from each other allows one to achieve nontrivial dynamics of the junction.

The results presented in the Chapter are the following: the non-topological Josephson junction demonstrates similar voltage staircase (sharp steps in average voltage for slowly changing current). In addition, there is a hysteresis curve - when current is slowly increased and then decreased, averaged voltage follow different path and the stairs appear at

different absolute values of current. Also there are found several minor distinctions from Majorana qubit behavior, which shows that Andreev levels do not fully mimic the topological qubit physics, but difference are hard to measure. To make effect observable the size of gaps should be not too small - which is different to typically studied systems with closed gap between levels.